This article has been accepted for publication in a future proceedings of this conference, but has not been fully edited. Content may change prior to final publication. Citation information: DOI10.1109/CISP-BMEIXXXXX2022.XXXXXXX, 2022 15th IEEE EMBS Regional Conference on Image and Signal Processing, BioMedical Engineering and Informatics (CISP-BMEI 2022)

Simultaneous Segmentation of Layers and Fluids in Retinal OCT Images

Nchongmaje Ndipenoch, Alina Miron, Zidong Wang and Yongmin Li
Department of Computer Science
Brunel University
Uxbridge, UB8 3PH, United Kingdom

***Abstract*—Accurate quantification of retinal Optical Coherence Tomography (OCT) images provides important clinical information of the pathological changes present in age-related macular degeneration (AMD). Currently, monitoring the progress of AMD is mostly performed manually by ophthalmologists, which is time-consuming, difficult and prone to errors. In this work, we have developed a model Deep_ResUNet++ to address this issue and to provide an automatic solution to the problem of simultaneous segmenting retinal layers and fluid regions from retinal OCT images. We have evaluated the method on the Annotated Retinal OCT Images (AROI) dataset. Experimental results demonstrate that our method outperformed the baseline U-Net model, the current state-of-the-art models (UNet_ASPP, ResUnet and ResUnet++) and even the human experts' annotation results, and achieved the best performance by a clear margin with Dice Score above 90% in every single class.**

I. Introduction

Age-related macular degeneration (AMD) is the most common cause of severe central vision impairment among patients over 50-years old in the developed world [7]. AMD can be classified as Dry AMD (also called atrophic AMD) which is less severe and more common, and Wet AMD (also called advanced neovascular AMD) which is the later stage of Dry AMD and is more severe and less common. Presently therapy with anti-vascular endothelial growth factor (anti-VEGF) is the main treatment for Dry AMD [1]. Ophthalmologists often advise the patients on behavioural changes such as diets and regular exercises which can help to slow down the progression and in some cases even lead to the prevention of the disease. Monitoring the progress of AMD is paramount, but so far this has been largely done manually, which is laborious and prone to errors. Optical Coherence Tomography (OCT), a cross-section scan of the retina with three dimensions, can provide high quality visualisations of the retinal layers with extensive information about the retinal anatomy. The development of an automatic method for analysing the retina structure from OCT images and therefore monitoring the progress of AMD will be of great importance.

To address the above issue, we present a model developed in this work, termed Deep_ResUNet++. As opposed to the common approach of treating retinal layers and fluid regions alone separately, we aim to provide an automatic solution for segmentation of both simultaneously.

The rest of the paper is organized as follows. A brief review of the previous studies is provided in Section II. Section III presents the proposed methods. The experiments and result analysis are presented in Section IV. Finally, the conclusion with our contributions is described in Sections V.

II. Background

Segmentation of retinal images has been of great interest for several decades. Various methods have been studied for this problem, from the traditional methods of graph-cut [17], [19], Markov Random Fields [18], [20], level set [3], [4], to the recent deep learning methods that will be briefly reviewed as below.

De Fauw et al [6] from Moorfields Eye Hospital NHS Foundation Trust London and DeepMind Health presented a framework for diagnosis and referral in retinal disease that consists of two parts, a segmentation model and a classification model. A three-dimensional U-Net architecture [22] was used in their segmentation model and the model was trained on 14,884 OCT scan volumes obtained from 7,621 patients.

Fang et al [5] reported an approach of automatic segmentation of nine retinal layer boundaries in OCT images of patients with dry AMD, where a regular Convolutional Neural Network (CNN) is used to extract the layer boundaries features from an input image and classify them into the nine classes representing the nine layer boundaries, and a graph search method to further classify the extracted features into ten classes using probabilistic methods so as to eliminate miss-classified features.

Another CNN-based approach is developed in [11] for retinal fluid segmentation and detection from OCT images. They build a framework to detect and segment three retinal fluids: Intraretinal fluid (IRF), subretinal hyperreflective material (SRF) and Retinal Pigment Epithelial Detachment (PED) in retinal OCT images using CNN. Their frame work consists of three main parts. The first part is to pre-process the image and segment the layers: Internal limiting membrane (ILM) and Retinal pigment epithelium (RPE) where the fluids are found, the second part is a two-dimension U-Net architecture used to extract the fluid features, and the third part is a Random Forest classifier which they used to classify the extracted features to further eliminate miss-classified features.

The ReLayNet architecture was presented in [16] for the segmentation of the layers and fluids in the OCT images. They used the Duke dataset which is publicly available. The dataset consists of 110 annotated B-scan (divided into 10 classes of 1

This article has been accepted for publication in a future proceedings of this conference, but has not been fully edited. Content may change prior to final publication. Citation information: DOI10.1109/CISP-BMEIXXXXX2022.XXXXXXX, 2022 15th IEEE EMBS Regional Conference on Image and Signal Processing, BioMedical Engineering and Informatics (CISP-BMEI 2022)

background, 8 layers and 1 fluid) acquired from ten patients suffering from Diabetic Macular Edema (DME).

Rashno et al [14] presented an approach to fluid segmentation in OCT images using neutrosophic transformation and a graph-based shortest path, and also evaluated with the DME dataset.

Other segmentation methods of the retinal structure using the OCT image modality includes [2], [9], [21].

Between the two most widely used network architectures of U-Net and CNN, previous studies indicate that the U-Net (two sided, encoder and decoder) tends to outperform CNN, and therefore in many applications U-Net is a preferred choice.

III. Method

A. *Deep_ResUNet++*

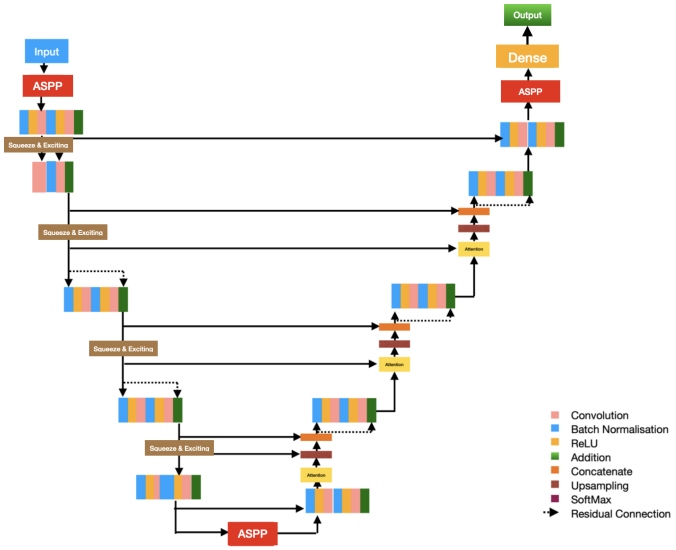

Fig. 1: Structure of Deep_ResUNet++.

The proposed model Deep_ResUNet++ is inspired and based on previous work ResUNet++ [8] but adapted to the specific problem of retina image segmentation. In the following, we will describe the architecture of the proposed model and explain the differences to the ResUNet++.

1) Encoding and Decoding Paths: The basic unit of the Deep_ResUNet++ is like the 2D U-Net architecture [15] with an encoding and decoding path. The encoder phase is used to capture local contextual information and the decoder phase to enable precise localization of the pixel with a bridge layer in between the encoder and decoder phases. The encoder is made up of five blocks and each block consists of three main parts or layers in sequence which are : batch normalization layer, the ReLU activation layer and the convolution layer. The batch normalization was used to prevent over-fitting during training, a rectangular kernel size of 7X3 was used to match the image dimension of 512X1024 instead of the square kernel size of 3X3 that was used in ResUNet++. Padding was set to zero to ensure that the feature map before and after the convolutional layer is the same. A stride of one was used to ensure there is no overlapping when constructing the feature map. The decoder is made up of five main parts or layers in sequence which are : batch normalization layer, the ReLU, the convolutional layer, the upsampling layer and the concatenating layer. The upsampling layer is used to capture spatial information from the feature map and the concatenating layer was used to concatenate images from the encoder phase to their corresponding decoder phase so that the size of the input image is the same as the output image, the three other layers were setup in the same way like in the encoder path. Before the encoding layer is an input layer that uses the Atrous Spatial Pyramid Pooling (ASPP) to capture global information and after the decoder layer is a classification layer that uses a SoftMax activation function to classify each of the pixel or voxel from the input feature map to belong to each of the 8 classes or labels. Unlike the ResUNet++ where a 2D convolutional layer was used, here we have used the dense layer as explained in III-A5.
The architecture of the proposed model is similar to ResUNet++ but is deeper (Deep_ResUNet++ has 5 convolutional blocks instead of 4 in ResUNet++) with an added convolutional layer in every convolutional block to efficiently deal with larger images.

2) The Bridge Layer: An Atrous Spatial Pyramid Pooling (ASPP) block is used as a bridge to the encoding and decoding phases. The ASSP is an up-sampled filtering technique use to capture global information in a feature map. It is comprised of multiple parallel atrous convolutional layers with different sampling rates. The ASPP blocks are designed for convolution with up-sampled filters, and are capable of capturing global contextual features or information and are also computationally efficient. Unlike ResUNet++ where 3 parallel filters with a dilation rate or frequency of 6, 12, and 18 were used in the Deep_ResUNet++ we have used 4 parallel filters with a dilating rate 6, 12, 18, and 24, this is because we have double the image capacity of the model therefore we also increases the model's capacity to capture global information. The introduction of the ASPP block is important for this problem because the number of fluid types found in the B-Scans varies (at least one fluid type was absent in some B-Scans). The ASPP block used in the Deep_ResUNet++ architecture is demonstrated in Fig. 2

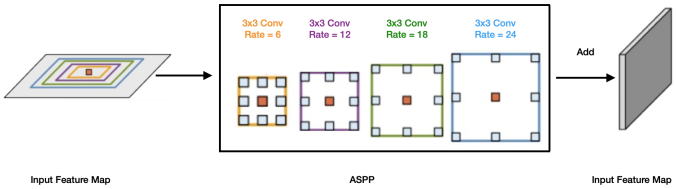

Fig. 2: The ASSP captures global information by employing multiple parallel filters with different rates.

3) Deep Residual Learning: In a neural network when adding more layers using certain activation functions like

This article has been accepted for publication in a future proceedings of this conference, but has not been fully edited. Content may change prior to final publication. Citation information: DOI10.1109/CISP-BMEIXXXXX2022.XXXXXXX, 2022 15th IEEE EMBS Regional Conference on Image and Signal Processing, BioMedical Engineering and Informatics (CISP-BMEI 2022)

Sigmoid (it squashes large input into smaller values between 0 and 1), the gradients of the loss function approaches zero. This will make the network difficult to train. In deep learning this problem is called the vanishing gradient problem. One way to circumvent this problem is to use the skip or residual connections, where some of the activation function layers are skipped during training, therefore reducing the number of times that the derivatives are squashed by the activation function. This is an important component in our model, because increasing the depth of the model will increase the likely-hood of the gradient problem to occur.

4) Squeeze and Exciting Block: The Squeeze and Exciting Block (SE) uses the Global Average Pooling (GAP) technique to capture global information by employing the average pooling method. In the encoding path as we transit from one convolutional block to another a GAP block is introduced between the blocks to capture global information. Here we have used GAP instead of ASPP because GAP has no parameter to optimize thus it is robust to overfitting as stated in section 3.2 of [10].

5) Dense Layer: Unlike the ResUNet++ where where 2D convolutions was used at the final layer of the decoding phase just before the output layer we have modified this to use the Dense layer in the Deep_ResUNet++, in order to learn and capture information from all the previous features. This increases the network's ability to capture global information and it is useful to this problem because the fluid regions demonstrate large degree of variation and are not as consistent as the retinal layers.

IV. Experiments

A. Dataset

The dataset used in the experiments is the Annotated Retinal OCT Images (AROI) database [12] collected using the Zeiss Cirrus HD OCT 4000. One OCT volume image of 128 B-scans from each of the 25 patients of wet AMD is included in the dataset, resulting a total of 3200 B-scans. Among the B-scans, 1136 from 24 patients are annotated and this is the subset we used in the experiments. The resolution of the B-scans is 1024 x 512 pixels (pixel size 1.96 x 11.74 μm).

In total 8 labels or classes were identified and the number of labels per B-Scan depend on the present or absence of fluids. Subretinal fluid, or subretinal hyperreflective material, (SRF/SRHM) and Intraretinal fluid (IRF) are not present in OCT volumes for all patients. SRF is not present in patients: 13, 17, and 19. SRF/SRHM are not present in patient: 3, 4, 6-9, 17, 20-22, and 24.

The B-Scans were labelled or annotated based on three categories which are layer, fluid and background. Historically the retinal OCT consists of 10 layers but for simplicity these layers are grouped into 3 distinct classes as follows: (1) Internal limiting membrane (ILM), which is the area between ILM and Inner plexiform layer and Inner nuclear layer (INL/IPL) boundaries, (2) Inner plexiform layer and Inner nuclear layer (IPL/INL), which is the area between the IPL/INL and Retinal pigment epithelium (RPE) boundaries, and (3) the Retinal pigment epithelium/Bruch's membrane complex (RPE/BM), which is the area between the RPE and BM boundaries. Four main retinal fluids were identified and categorized into 3 classes or labels as follows: (1) The Intraretinal fluid (IRF), (2) the Subretinal fluid and subretinal hyperreflective material (identified as SRF as they are in the same location), and (3) the Retinal Pigment Epithelial Detachment (PED). Two backgrounds were identified and categorized into 2 classes as follows: (1) the area above Internal limiting membrane (ILM) and (2) the area below the Bruch's membrane (BM).

The classes are coloured as follow: Black is the area above ILM, red is the ILM layer, yellow is the area between the IPL and INL layers, white is the the RPE and BM layers, blue is the area under the BM, Light Blue is the PED fluid, Pink is the SRF/SRHM fluids and green is the IRF. An example of labelling and annotation of classes of both retinal layers and fluids is shown in Fig. 3.

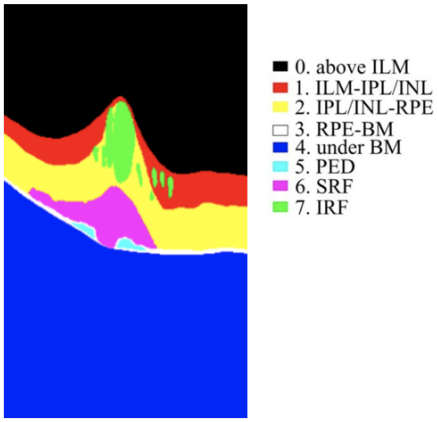

Fig. 3: An example of annotation of the layers and fluids in the AROI dataset.

The AROI dataset is particularly interesting because it was collected for two problems - retinal layer segmentation and fluid segmentation. To the best of our knowledge as of now AROI is the only publicly available retinal OCT dataset with more than one layer and more than one fluid with annotations. To add to the complexity of the problem, the dataset is also highly imbalanced. Out of the 1136 annotated B-scans, PED, SRF, and IRF are present in 1014 (89.26%), 648 (57.04%), and 229 (20.16%) B-scans, respectively.

B. Training and Testing

It is a common practice to separate the segmentation of regular retinal layers and detection of fluids, but in this work we aim to perform both tasks simultaneously.

K-fold cross validation was used for training, validation and testing. For fair comparison, we used the same data splits as in the baseline model [13]: Each fold consists of B-scans from 4 patients. For examples, the first fold consists of patient 1,2,3 and 4, and then patient 5,6,7 and 8 for the second fold and so on. Splitting B-scans from the same patient across training, validation, and test is not recommended as adjacent

This article has been accepted for publication in a future proceedings of this conference, but has not been fully edited. Content may change prior to final publication. Citation information: DOI10.1109/CISP-BMEIXXXXX2022.XXXXXXX, 2022 15th IEEE EMBS Regional Conference on Image and Signal Processing, BioMedical Engineering and Informatics (CISP-BMEI 2022)

B-scans are similar and that could lead to bias. The test set is approximately 15% of the dataset. For all the experiments the following parameters were set as follows, again, the same as in the baseline study: the value of k was 6, the original image size of 1024 × 512 pixels, the loss function used was Categorical cross-entropy, the batch size was set to 4, AdaBound was the optimizer used, the learning rate was 0.001 and early stopping was used to prevent overfitting.

Dice score was the evaluation metric used to measure the performance of the algorithm. It is a similarity measure often used as a metric in the segmentation of medical images. The Dice Score is the percentage of pixels or voxels in an image that is classified correctly per class or segment. It is calculated by taking twice the intersection and dividing it by the union for each class or segment as in Eqn (1).

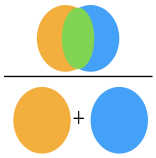

$$DSC = \frac{2|X \cap Y|}{|X| + |Y|} \quad (1)$$

The Dice Score was calculated per patient in the test fold (4 patients per fold) and the mean value of the patients per fold was taken but only for patients with segmentation reference. At least one of the IRF and SRF fluids are missing in some patients (both fluids were missing in patient 17, and one fluid is missing in patient 3, 9, 13, 16, 20, 21, 22, and 24). Therefore, during testing, patents with whom at least one fluid is missing in the B-scans the Dice Score was exempted for that class and that patient in other to avoid over estimation or under estimation. In patients with whom at least one fluid is missing in some B-scan but not all of them, the Dice Score was set to zero. The Dice Score was calculated per patient because mixing adjacent B-sans of the same patients with other patients will lead to over estimation.

The models were trained on a GPU Server with NVIDIA RTX A6000 48GB. The models were implemented in Python, using the Keras library with the TensorFlow backend.

C. Results

In this section we report the performance measured by the Dice Score for each segment classes and each methods including the Inter-observer, the baseline U-Net, the proposed Deep_ResUnet++ and other state-of-the-art architectures (UNet_ASPP, ResUnet and ResUnet++) in this domain. The segmentation performance grouped by segment classes is illustrated in Fig. 4, and all the Dice Scores in Table I. From these results, we notice the following:

1) The proposed model Deep_ResUnet++ outperforms the human experts, the baseline (U-Net) and current state-of-the-art models (UNet_ASPP, ResUnet and ResUnet++) in very single class with a Dice Score above 90%.
2) The IRF class was the most difficult to segment with the Deep_ResUnet++ achieving a Dice Score of 91% which is 11.5% higher than that archived by the second best Model, ResUnet++ for that class.
3) It is observed an increase of performance from the standard U-Net to more complex architectures in the order of UNet_ASPP, ResUnet, ResUnet++ and Deep_ResUnet++.
4) It is also observed that the Deep_ResUnet++ obtained an overall mean Dice Score of 98% which is 10% higher than that of the human experts' annotation results of 88%.
5) The Dice score of the background classes and the layer (except the RPE/BM) classes were always very high for all the models. This was expected as the background classes occupy most of the image, and the two other layers except RPE/BM are made up of three or more thick retinal layers as oppose to the RPE/BM which is made up of two thin retinal layers.

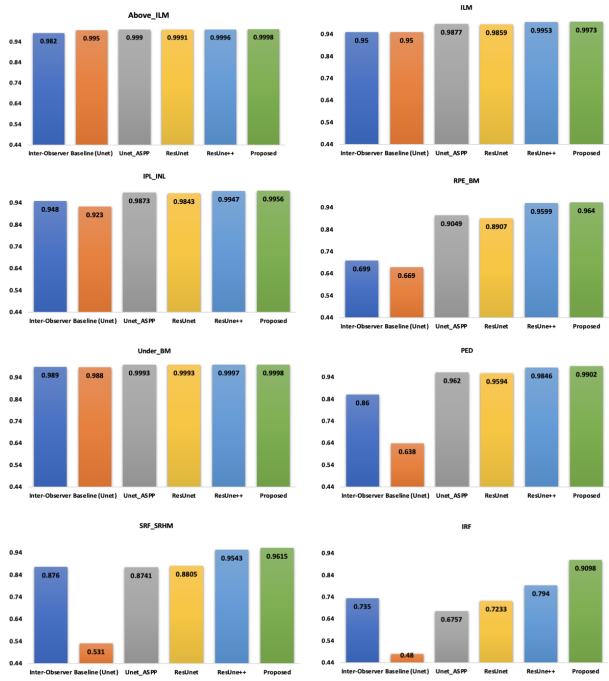

Fig. 4: Performance comparison (measured by the Dice scores) of the proposed method of Deep_ResUnet++, together with the baseline U-Net model, the Inter-Observer (by human experts) and other state of the arts models: UNet_ASPP, ResUnet and ResUnet++ in this domain. The results are grouped by the segment classes.

TABLE I: Table of the Dice Scores by segment classes (rows) and models (columns).

	Inter_Ob.	Baseline	UNet_ASPP	ResUNet	ResUNet++	**Proposed**
Above_ILM	0.9820	0.9950	0.9990	0.9991	0.9996	**0.9998**
ILM	0.9500	0.9500	0.9877	0.9859	0.9953	**0.9973**
IPL_INL	0.9480	0.9230	0.9873	0.9843	0.9947	**0.9956**
RPE_BM	0.6990	0.6690	0.9049	0.8907	0.9599	**0.9640**
Under_BM	0.9890	0.9880	0.9993	0.9993	0.9997	**0.9998**
PED	0.8600	0.6380	0.9620	0.9594	0.9846	**0.9902**
SRF_SRHM	0.8760	0.5310	0.8741	0.8805	0.9543	**0.9615**
IRF	0.7350	0.4800	0.6757	0.7233	0.7940	**0.9098**

This article has been accepted for publication in a future proceedings of this conference, but has not been fully edited. Content may change prior to final publication. Citation information: DOI10.1109/CISP-BMEIXXXXX2022.XXXXXXX, 2022 15th IEEE EMBS Regional Conference on Image and Signal Processing, BioMedical Engineering and Informatics (CISP-BMEI 2022)

Examples of the segmentation results are shown in Fig. 5 together with the original input images and their annotations.

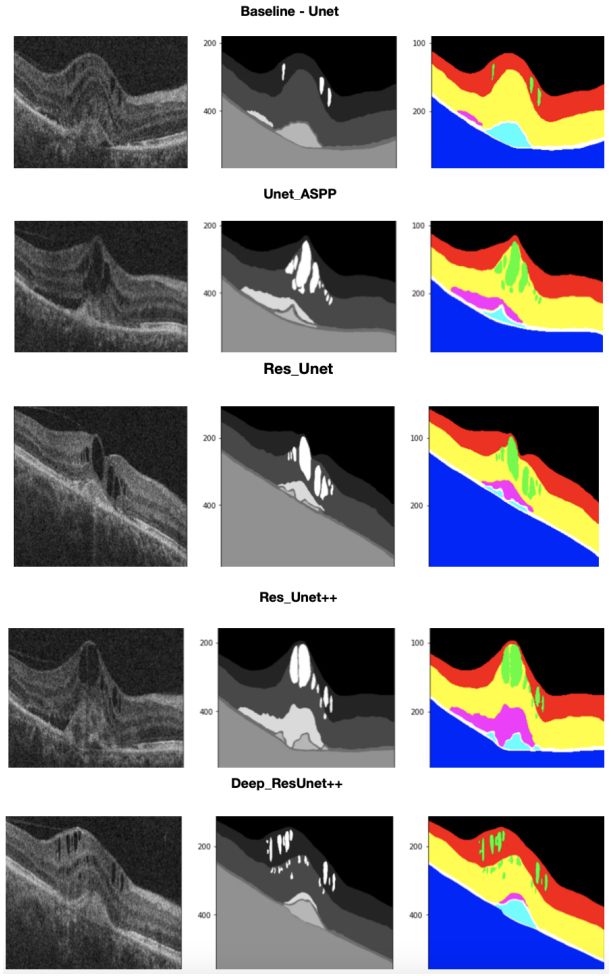

Fig. 5: Examples of segmentation results, from left to right, the inputs, annotations and outputs for the Baseline Unet, the three state-of-the-arts models and the proposed Deep_ResUnet++.

V. Conclusions

In this work, we have investigated the problem of simultaneous segmentation of both retinal layers and fluid regions from OCT retinal images. Based on the previous studies of [8] and taking into considerations of the specific problem of retina image segmentation, a new model named the Deep_ResUnet++, was developed and evaluated on the AROI dataset. Experimental results show that our proposed method outperformed the baseline U-Net method, other state of the arts methods (UNet_ASPP, ResUnet and ResUnet++) in this domain and even the human experts results by a clear margin.

It is important to note that, instead of separating the two problems of retinal layer segmentation and fluid region segmentation alone, our model is designed to segment both simultaneously and therefore it is a much more challenging task. In addition, the chosen dataset AROI is highly imbalanced which further adds to the complexity of the problem.

The method presented in this work can be directly applied for structure analysis of OCT retinal images and further monitoring the progress of eye diseases such as AMD. In the future, we will investigate the performance of this method on other datasets once they are publicly available. Also we will look into extending the models from the current two-dimensional architecture to three-dimensional.

References

[1] David Brown, Jeffrey Heier, David Boyer, K. Freund, Peter Kaiser, Judy Kim, and David Sarraf. Current best clinical practices—management of neovascular amd. *Journal of VitreoRetinal Diseases*, 1:247412641772594, 08 2017.

[2] Stephanie Chiu, Michael Allingham, Priyatham Mettu, Scott Cousins, Joseph Izatt, and Sina Farsiu. Kernel regression based segmentation of optical coherence tomography images with diabetic macular edema. *Biomedical Optics Express*, 6, 04 2015.

[3] Bashir Isa Dodo, Yongmin Li, Djibril Kaba, and Xiaohui Liu. Retinal layer segmentation in optical coherence tomography images. *IEEE Access*, 7:152388–152398, 2019.

[4] Bashir Isa Dodo, Yongmin Li, and Xiaohui Liu. Level set segmentation of retinal oct images. In *International Conference on Bioimaging. Czech Republic.*, 2019.

[5] Leyuan Fang, David Cunefare, Chong Wang, Robyn H Guymer, Shutao Li, and Sina Farsiu. Automatic segmentation of nine retinal layer boundaries in oct images of non-exudative amd patients using deep learning and graph search. *Biomedical optics express*, 8(5):2732–2744, 2017.

[6] Jeffrey Fauw, Joseph Ledsam, Bernardino Romera-Paredes, Stanislav Nikolov, Nenad Tomasev, Sam Blackwell, Harry Askham, Xavier Glorot, Brendan O'Donoghue, Daniel Visentin, George Driessche, Balaji Lakshminarayanan, Clemens Meyer, Faith Mackinder, Simon Bouton, Kareem Ayoub, Reena Chopra, Dominic King, Alan Karthikesalingam, and Olaf Ronneberger. Clinically applicable deep learning for diagnosis and referral in retinal disease. *Nature Medicine*, 24, 09 2018.

[7] https://www.nei.nih.gov/learn-about-eye-health/eye-conditions-and-diseases/age-related-macular degeneration.

[8] Debesh Jha, Pia H Smedsrud, Dag Johansen, Thomas de Lange, Håvard D Johansen, Pål Halvorsen, and Michael A Riegler. A comprehensive study on colorectal polyp segmentation with resunet++, conditional random field and test-time augmentation. *IEEE journal of biomedical and health informatics*, 25(6):2029–2040, 2021.

[9] Cecilia S Lee, Ariel J Tyring, Nicolaas P Deruyter, Yue Wu, Ariel Rokem, and Aaron Y Lee. Deep-learning based, automated segmentation of macular edema in optical coherence tomography. *Biomedical optics express*, 8(7):3440–3448, 2017.

[10] Min Lin, Qiang Chen, and Shuicheng Yan. Network in network. *arXiv preprint arXiv:1312.4400*, 2013.

[11] Donghuan Lu, Morgan Heisler, Sieun Lee, Gavin Ding, Marinko V Sarunic, and Mirza Faisal Beg. Retinal fluid segmentation and detection in optical coherence tomography images using fully convolutional neural network. *arXiv preprint arXiv:1710.04778*, 2017.

[12] M Melinščak, M Radmilovič, Z Vatavuk, and S Lončarić. Aroi: Annotated retinal oct images database. In *2021 44th International Convention on Information, Communication and Electronic Technology (MIPRO)*, pages 371–376. IEEE.

[13] Martina Melinscak, Marin Radmilović, Sven Loncaric, and Zoran Vatavuk. Annotated retinal optical coherence tomography images (aroi) database for joint retinal layer and fluid segmentation. *Automatika*, 62:375–385, 08 2021.

[14] Abdolreza Rashno, Dara D Koozekanani, Paul M Drayna, Behzad Nazari, Saeed Sadri, Hossein Rabbani, and Keshab K Parhi. Fully automated segmentation of fluid/cyst regions in optical coherence tomography images with diabetic macular edema using neutrosophic sets and graph algorithms. *IEEE Transactions on Biomedical Engineering*, 65(5):989–1001, 2017.

[15] Olaf Ronneberger, Philipp Fischer, and Thomas Brox. U-net: Convolutional networks for biomedical image segmentation. In *International Conference on Medical image computing and computer-assisted intervention*, pages 234–241. Springer, 2015.

This article has been accepted for publication in a future proceedings of this conference, but has not been fully edited. Content may change prior to final publication. Citation information: DOI10.1109/CISP-BMEIXXXXX2022.XXXXXXX, 2022 15th IEEE EMBS Regional Conference on Image and Signal Processing, BioMedical Engineering and Informatics (CISP-BMEI 2022)

[16] Abhijit Guha Roy, Sailesh Conjeti, Sri Phani Krishna Karri, Debdoot Sheet, Amin Katouzian, Christian Wachinger, and Nassir Navab. Relaynet: retinal layer and fluid segmentation of macular optical coherence tomography using fully convolutional networks. *Biomedical optics express*, 8(8):3627–3642, 2017.

[17] Ana Salazar-Gonzalez, Djibril Kaba, Yongmin Li, and Xiaohui Liu. Segmentation of the blood vessels and optic disk in retinal images. *IEEE journal of biomedical and health informatics*, 18(6):1874–1886, 2014.

[18] Ana Salazar-Gonzalez, Yongmin Li, and Djibril Kaba. MRF reconstruction of retinal images for the optic disc segmentation. In *International Conference on Health Information Science*, pages 88–99, 2012.

[19] Ana G Salazar-Gonzalez, Yongmin Li, and Xiaohui Liu. Retinal blood vessel segmentation via graph cut. In *International Conference on Control Automation Robotics & Vision*, pages 225–230, 2010.

[20] Chuang Wang, Y Wang, and Yongmin Li. Automatic choroidal layer segmentation using markov random field and level set method. *IEEE journal of biomedical and health informatics*, 2017.

[21] Jie Wang, Miao Zhang, Alex D Pechauer, Liang Liu, Thomas S Hwang, David J Wilson, Dengwang Li, and Yali Jia. Automated volumetric segmentation of retinal fluid on optical coherence tomography. *Biomedical optics express*, 7(4):1577–1589, 2016.

[22] Özgün Çiçek, Ahmed Abdulkadir, Soeren Lienkamp, Thomas Brox, and Olaf Ronneberger. 3d u-net: Learning dense volumetric segmentation from sparse annotation. 06 2016.